Nanoscale Res Lett (2010) 5:1307–1312
DOI 10.1007/s11671-010-9643-9

NANO EXPRESS

On the Morphology, Structure and Field Emission Properties of Silver-Tetracyanoquinodimethane Nanostructures

Chunnuan Ye · Kaibo Zheng · Wenlong You · Guorong Chen

Received: 22 April 2010 / Accepted: 7 May 2010 / Published online: 22 June 2010

Abstract Silver-tetracyanoquinodimethane(Ag-TCNQ) nanostructured arrays with different morphologies were grown by an organic vapor-transport reaction under different conditions. The field emission properties of nanostructured arrays were studied systematically. Their morphology and crystal structure were characterized by SEM and XRD, respectively. It was found that the field emission properties were strongly dependent on the reaction temperature and the initial Ag film thickness. The lowest turn-on field with 10-nm-thick silver film is about 2.0 V/μm, comparable to that of carbon nanotubes. The film crystal structure and the morphology are contributed to the final emission performance.

Keywords Organic semiconductor · Nanostructures · Ag-TCNQ · Field emission

Introduction

Field emission is of considerable interest over the past few years. Especially, various kinds of conventional inorganic semiconductors have been considered as promising field emitters to fabricate field emission displays because of their high enhancement factor, physical and chemical properties and wide range of possible applications [1]. However, organic nanostructured materials are scarcely reported on the field emission properties. Tris (8-hydroxyquinoline) aluminum (Alq) [2], copper hexadeca fluorophthalocyanine ($F_{16}CuPc$) [3], CuPc [3], copper/silver tetrafluoro tetracyanoquinodimethane (CuTCNQF$_4$) and AgTCNQF$_4$ [4] have been reported. It is especially notable for the M-TCNQF$_4$ nanostructures, which exhibit tunable morphologies, high current density and low turn-on field. But the growth temperature of M-TCNQF$_4$ nanostructures is higher than 443 K. M-TCNQ one-dimensional (1D) nanostructures grown at a lower reaction temperature have attracted enormous attention due to their electrical switching effect for memory device application [5], and large area [6] and enhanced field emission by a metal buffer layer [7] are reported. It is better for device on those flexible substrates that the reaction temperature is relatively low.

However, it is still elusive to understand the relations between the growth conditions and the emission properties due to the complex shape and crystalline structure; defects and interface states. So in this paper, the dependence of field emission from Ag-TCNQ nanowires on different growth conditions including reaction temperature, starting silver film thickness and reaction time span were studied and discussed according to SEM and XRD characterizations of the Ag-TCNQ nanostructures in detail.

Experimental

The samples were produced via a vacuum vapor-transport reaction method developed in our previous work [8]. First,

C. Ye (✉)
College of Chemistry, Chemical Engineering and Materials Science, Soochow University, 215123 Suzhou, People's Republic of China
e-mail: cnye@suda.edu.cn

K. Zheng · G. Chen (✉)
Department of Chemistry, Fudan University, 200433 Shanghai, People's Republic of China
e-mail: grchen@fudan.edu.cn

W. You
School of Physical Science and Technology, Soochow University, 215006 Suzhou, Jiangsu, People's Republic of China

Ag film was thermal evaporated on substrate with base pressure of 2×10^{-3} Pa and thickness monitored by an in situ microbalance of quartz crystal. The metal film on the substrate together with TCNQ powder (98%, Aldrich) was then placed in a quartz tube connected to a vacuum chamber. After pumping down to 2×10^{-3} Pa, the quartz tube was sealed and thermal treated in the furnace. After reacting for some time, the blue-colored film covered on the substrate was prepared and then taken out for subsequent experiments.

To study the field emission properties of Ag-TCNQ nanostructures, the morphologies characterization for those samples grown under different conditions is necessary. The morphology is characterized by scanning electron microscopy (SEM, XL30FEG,PHILIPS, with a resolution of 2 nm). The structure of the as-grown nanostructures is by X-ray diffraction (XRD, Rigaku D/Max-3C).

Field emission measurements were carried out in a parallel-plate configuration with the base pressure of 5×10^{-3} Pa in a vacuum chamber. The nanostructures sample acted as the cathode, and a steel cylindrical electrode acted as the anode. In this study, the turn-on field is defined as the applied electric field that can generate a current density of 10 μA/cm^2. The cross-sectional area of the anode is 0.498 cm^2 defined as the field emission area to obtain the current density.

Results and Discussion

Figure 1 shows the typical top view of the as-deposited Ag-TCNQ nanowires at 393 and 423 K. As a whole, most of them are vertical to the substrate with a sharp tip. The diameter varies from 50 to 150 nm.

Figure 2 shows the top view for samples with 10, 30 and 50-nm-thick silver films. It is shown that the density of the nanowires becomes larger, and the orientation perpendicular to the substrate becomes more regular with the increase in the film thickness. As shown in the left Fig. 2a, sparse nanowires are aligned irregularly, reclining or lying. More nanowires will grow and align more perpendicular to the substrate due to the space limit effect in a thicker silver film. For the samples with 30-nm-thick Ag film, the nanowires are with obviously sharp tips, but the tips are not like that with 50-nm Ag film. Because thicker Ag film will give more and smaller particles upon heating, and higher rate of diffusion dominates, the nanowires grow seemingly in succession without obvious tips on the surface.

In addition, the thickness of silver film greatly influences the length of as-obtained nanowires. Actually, the length of the nanowire depends on the thickness as well as the growth time. Given that the growth reaction is completed, we observe that the thickness of the pre-deposited Ag film actually dominates the length of Ag-TCNQ nanowires from the side-view SEM image of as-obtained nanowires. First, as the Ag^+ source for nanowire growth is derived from the pre-deposited Ag film, the thicker film will provide larger amount of Ag source, which would extend the reaction time in the process of nanowire growth, thus Ag-TCNQ with larger length could form. In short, the thickness of the pre-deposited film is proportional to the length of as-obtained nanowire. However, when the thickness is rather high (etc. μm order), the film is unlikely to melt into molten droplets within the thermal treatment. Therefore, the VS growth process would be inhabited resulting in the absence of nanowire to synthesize. The same results can also be obtained with regard to Cu-TCNQ counterpart.

In our experiments, XRD patterns of the as-prepared Ag-TCNQ at different reaction temperature are shown in Fig. 3. Those patterns for samples grown at 363 K are indexed similar to that orthorhombic structure [9] with $a = 6.975$ Å, $b = 16.686$ Å, $c = 17.455$ Å and $V = 2031.5$ Å^3, named phase II. In the sample grown at 373 K, most of phase I is

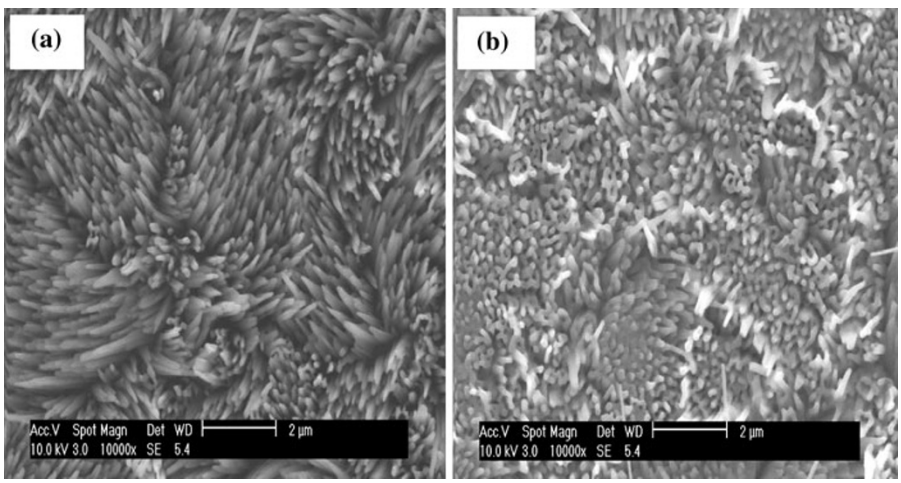

Fig. 1 SEM *top-view* images of Ag-TCNQ nanowires, with 30 nm Ag film at 393 and 423 K, respectively

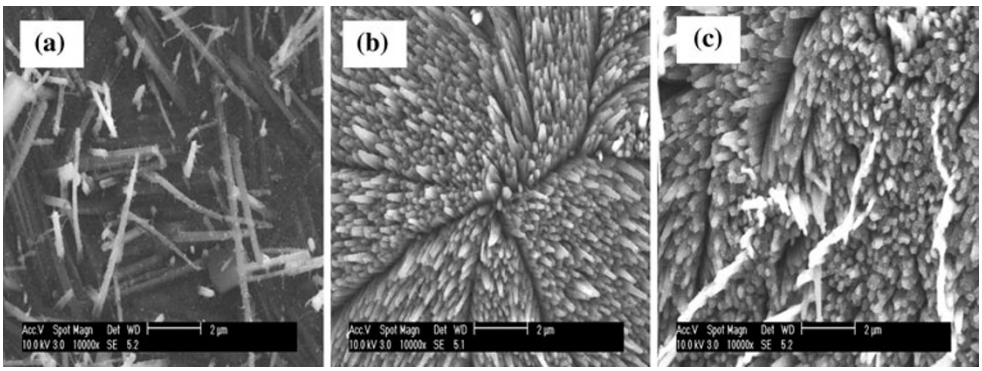

Fig. 2 SEM *top-view* images of Ag-TCNQ nanowires, with 10, 30 and 50-nm-thick Ag film at 413 K, respectively

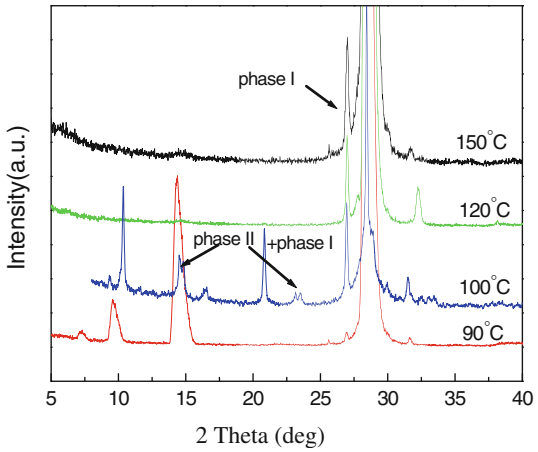

Fig. 3 XRD patterns of Ag-TCNQ nanostructures on Si, substrate under different temperatures, respectively

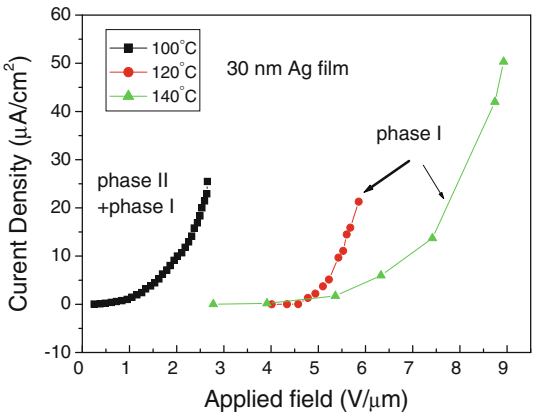

Fig. 4 *J–E* curves of field emission for Ag-TCNQ nanowires, grown at different temperature

consisted with three preferential growth directions and still mixed some phase II. And the other samples grown at a temperature higher than 393 K are indexed to that tetragonal cell with $a = b = 12.142$ Å, $c = 17.049$ Å and $V = 2513.7$ Å^3, named phase I, whose structure remains constant but the preferential growth direction changes a little from larger to smaller diffraction angle with the reaction temperature from 393 to 413 K. These results indicate that the growth of Ag-TCNQ crystals is sensitive to the reaction temperature.

Because the Ag-TCNQ nanowires with 30-nm-thick Ag film are with regular array and proper structure of tips, their field emission properties dependence on the other growth conditions are first studied in detail. Figure 4 shows the characteristics of emission current density versus applied field for them grown under the reaction temperature of 373, 393 and 413 K with 30-nm-thick Ag film, respectively, and other conditions are the same. With the temperature increasing, the turn-on field is 2.0, 5.5 and 7.0 V/μm, respectively. The turn-on field for the former one is lower than that of the latter two, mainly because they consist of different crystalline structures recognized by the XRD analysis shown in Fig. 3. The former one belongs to phase II mixed with some of phase I and the others completely to phase I. From this point, we can conclude that the phase I grown under higher temperature has higher resistivity than the phase II for the former one.

Because high preferential growth happens under high reaction temperature, the field emission tests for those Ag-TCNQ nanowires grown under 413 K with 10, 30 and 50-nm-thick Ag film are shown in Fig. 5a, b, respectively. It is shown that the turn-on field is 11.5, 9.3 and 13.5 V/μm, respectively, with the increasing of thickness. Since the samples are grown under the same temperature, the crystal structure is the same phase I. The difference in field emission mainly depends on the morphology of nanowires array. From the corresponding SEM images in Fig. 2 maybe some defects exist on the side of the nanowires in Fig. 2a. No enough tips are contributed to the field emission. While too many nanowires align parallel in Fig. 2c, the field enhancement factor is smaller resulting from the reduced local field on the tips, due to the screening effect. So we can conclude that both the morphology and proper density of

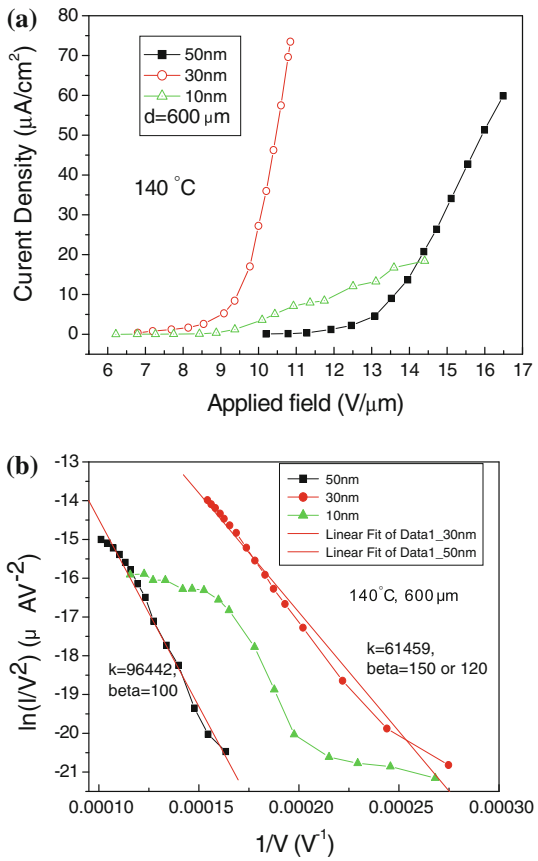

Fig. 5 **a** *J–E* curves of field emission for Ag-TCNQ nanowires grown with 10, 30 and 50-nm-thick Ag film, the gap distance between electrodes d is 600 μm, **b** Field emission corresponding F–N curves for Ag-TCNQ nanowires, with different Ag film thickness

nanowires are contributed to the lowest turn-on field for the samples in Fig. 2b.

In order to analyze the origin of field emission from nanostructures, the revised Fowler–Nordheim(F–N) model is often used. If the plot of (ln (J/E^2) vs. 1/E *or* ln (I/V^2) vs. 1/V) yields a straight line, it implies that a quantum tunneling process is responsible for the field emission. The slope of the F–N plot can be expressed as [10]:

$$\text{slope} = -\frac{B\Phi^{3/2}}{\beta} \tag{1}$$

or

$$\text{slope} = -\frac{B\Phi^{3/2}d}{\beta} \tag{2}$$

where B is the constant of 6.83×10^3, d is the vacuum gap distance between electrodes. Three F–N plots of Ag-TCNQ nanowires grown with different thickness of Ag film are given in Fig. 5a corresponding to the *J-E* curves in Fig. 5b. In the middle curve for sample with the 10-nm-thick Ag film, the nonlinearity is obvious; but both of the others show a good line with almost the same slope. The following are the reasons for the nonlinearity. First, from the corresponding SEM images in Fig. 2a, there are many nanowires lying on the substrate. The side of Ag-TCNQ nanowire acts as emitters, some defects (adsorbates) on the side may first emit the electrons. Its field enhancement factor is different from the tip of nanowires in the other two samples. Second, different enhancement factors appear in different field regions. In the low field region, these defects have larger enhancement factor, resulting in a lower slope. With the increase in the field, the defects become less and at the same time some nanowires with smaller factor than that of those defects contribute to the emission current. As a result, higher slope appears in this field region. With the field further increasing, smaller slope results from both lying and vertical wires with little defects. Semet [11] reported that the linearity of F–N plot can be obtained by desorbing by applying the field for long time. It can be reduced that the defects (adsorbate) in the body of emitters result in the emission current and then the nonlinear F–N plot. Other nonlinearity in nanomaterials is reported either and discussed [12, 13].

Allowing for the switching effect for single M-TCNQ nanowires at the order of V/μm [13], identical to the applied field for emission, it is necessary to consider the effect during the field emission process. To study the process of field emission for Ag-TCNQ nanostructured arrays, XRD analysis was used to characterize the crystal structure of the samples after the field emission test. It is shown in Fig. 6a. From comparison with the patterns for samples as-grown in Fig. 1, this sample after emission at the high field regions gives XRD peaks locating at 2theta equal to 38.52 and 44.60 indexing for Ag(111) and (200), i.e., showing the same switching effect from single Ag-TCNQ nanowire. After the applied field reaches the value of turn-on field, the switching happens, and as a result the lower resistivity of the nanostructured array shows good field emission property with higher current density.

Figure 6b, c shows the *I-E* curves and corresponding F–N plots for sweeping emission from Ag-TCNQ nanowires with 30-nm-thick Ag film. The *I-E* curves in Fig. 6b almost remain coincident, but the corresponding F–N plots for them are not in complete agreement especially in low field region shown in Fig. 6c. These F–N plots are separated with low and high field regions for each sweeping process. The intercedes of the F–N plots in y-axis are equal, suggesting that the emission area in this high field region not changed, and the stability of field emission is high. The slopes and intercedes of these plots in the high field region are the same, showing the effective emission area and the emission for the Ag-TCNQ nanowires constant and stable.

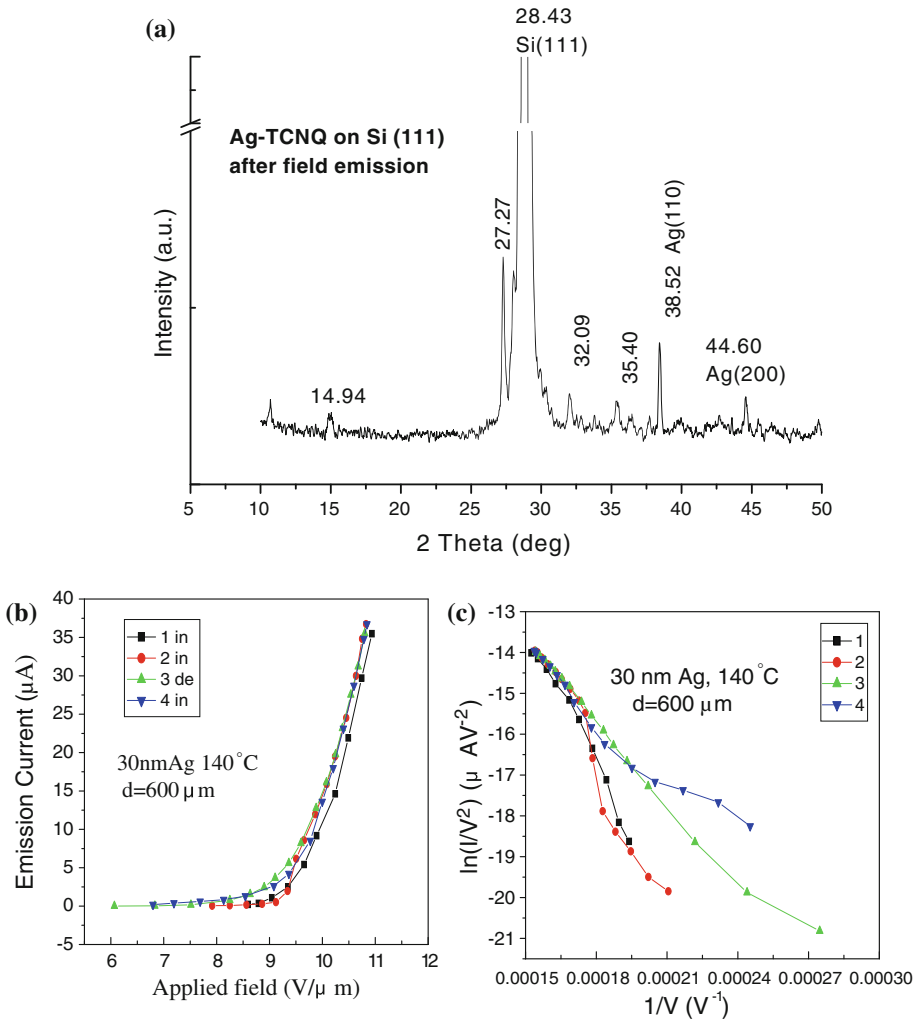

Fig. 6 **a** XRD patterns for Ag-TCNQ nanowires after field emission, **b** *I-E* curves of field emission for Ag-TCNQ nanowires by sweeping field tests, **c** F–N curves for Ag-TCNQ nanowires corresponding to **b**

Those different nanostructures array with some certain morphology have different field enhancement factor and effective work function. From the Eq. 2, we can estimate the work function by supposing properly a given field enhancement factor and evaluating the slope of the F–N plots in Fig. 6c. For those grown with 30-nm-thick Ag films in Fig. 2, the length maximum of nanowires is supposed to be about 10 μm, and the diameter is about 100 nm combined with SEM images.

Allowing for the electrical switching effect, the first decreasing the field is the process of recovery of Ag-TCNQ with high competence. If the field enhancement factor being 150 and 120 for Ag-TCNQ nanowires, respectively, the local effective work function for Ag-TCNQ nanowires in form of phase I can be derived to be 1.71 and 1.48 eV, respectively according to the slope of plot 3 in Fig. 6c. The work function for Ag-TCNQ nanowires grown with the initial 50-nm-thick Ag film is derived similarly to be 1.77 eV with the value of field enhancement factor being 100 in Fig. 5b. So the work function for the Ag-TCNQ nanowires array is smaller than 1.77 eV.

Properties comparison of field emission from other organic materials is listed in the Table 1 for comparison. Although the turn-on field is higher in our tests, but the lower work function shows the potential application in Organic FEDs. The lower temperature will produce the Ag-TCNQ phase II with lower turn-on field. And the main point for good field emission lies on the high conductivity and the regular array density. Further work needs to be done to verify the difference between two phases and to improve the field emission property of Ag-TCNQ. Perhaps, copper tetra-cyanoquinodimethane(Cu-TCNQ) nanowires are worth to be studied because much higher conductivity in bulk materials exists [14]. Moreover, recent work on the single Cu-TCNQ nanowire shows that the threshold field for the switching effect is about 1.2 V/μm [5], which is lower than that of single Ag-TCNQ nanowire being 9.3 V/μm [15].

Table 1 Properties comparison of some organic materials for field emission

Materials	Vacuum gap (μm) (thickness)	Turn-on field (V/μm)	Work function (eV)	Ref.
Ag-TCNQ	600 (50 nm Ag)	13.5	1.77	Our work
Ag-TCNQ	600 (30 nm Ag)	9.3	1.71 or 1.48	Our work
Ag-TCNQ	(foil)	2.58	1.19	Ref. [6]
Cu-TCNQ	(foil)	3.13	2.77	Ref. [6]
F16CuPc		9.3,9.8,12.7	5.1	Ref. [3]
CuPc		8.7(alfa) 8.1(beta) 9.7(alfa + beta)	4.62	Ref. [3]
F4TCNQ-Ag	300 (foil)	5.21	1.07	Ref. [4]
F4TCNQ-Cu	300 (foil)	5.48	2.39	Ref. [4]
AlQ3		10	3	Ref. [2]

Conclusions

In conclusion, the field emission properties for Ag-TCNQ nanostructured array were dependent on the structure and morphology determined by the reaction temperature and the initial Ag film thickness. The turn-on field to generate a density of 10 μA/cm^2 increases with the growth temperature from 373 to 413 K, and the lowest turn-on field obtained is about 2.0 V/μm for phase II. The deviation from the F–N linear relation may result from the difference of field enhancement factors at high and low field region, not excluding the emission from the surface defects in the nanowires in the low field region. The effective work function of Ag-TCNQ phase I nanowires array is estimated to be about 1.77 eV at most, which is lower among the organic materials.

Acknowledgment This work is supported financially both by NSFC (60471010, 60976050) and Postdoctoral Science Foundation of Jiangsu (0901082C).

References

1. X. Fang, Y. Bando, U.K. Gautam, C. Ye, D. Golberg, J. Mater. Chem. **18**, 509 (2008)
2. J.J. Chiu, C.C. Kei, T.P. Perng, W.S. Wang, Adv. Mater. **15**, 1361 (2003)
3. W.Y. Tong, Z.X. Li, A.B. Djurisic, W.K. Chan, S.F. Yu, Mater. Lett. **61**, 3842 (2007)
4. C. Ouyang, Y. Guo, H. Liu, Y. Zhao, G. Li, Y. Li, Y. Song, Y. Li, J. Phys. Chem. C. **113**, 7044 (2009)
5. K.B. Zheng, H.T. Shen, C.N. Ye, J.L. Li, D.L. Sun, G.R. Chen, Nano-Micro. Lett. **1**, 23–26 (2009)
6. H. Liu, Q. Zhao, Y. Li, Y. Liu, F. Lu, J. Zhuang, S. Wang, L. Jiang, D. Zhu, D. Yu, J. Am. Chem. Soc. **127**, 1120 (2005)
7. K. Zheng, X. Li, X. Mo, G. Chen, Z. Wang, G. Chen, Appl. Surf. Sci. **256**, 2764 (2010)
8. Y. Chun-Nuan, C. Guan-Ying, M. Xiao-Liang, F. Fang, X. Xiao-Yan, C. Guo-Rong, S. Da-Lin, Chin. Phys. Lett. **21**, 1787 (2004)
9. S.A. O'Kane, R. Clérac, H. Zhao, X. Ouyang, J.R. Galán-Mascarós, R. Heintz, K.R. Dunbar, J. Solid. State. Chem. **152**, 159 (2000)
10. R.G. Forbes, K.L. Jensen, Ultramicroscopy **89**(1–3), 17 (2001)
11. V. Semet, V.T. Binh, P. Vincent, D. Guillot, K. Teo, M. Chhowalla, G. Amaratunga, W.I. Milne, P. Legagneux, D. Pribat, Appl. Phys. Lett. **81**, 343 (2002)
12. Y. Chen, S.Z. Deng, N.S. Xu, J. Chen, X.C. Ma, E.G. Wang, Mater. Sci. Eng. A **327**, 16 (2002)
13. N.S. Xu, J. Chen, S.Z. Deng, Appl. Phys. Lett. **76**, 2463 (2000)
14. R.A. Heintz, H. Zhao, X. Ouyang, G. Grandinetti, J. Cowen, K.R. Dunbar, Inorg. Chem. **38**, 144 (1999)
15. Z.Y. Fan, X.L. Mo, G.R. Chen, J.G. Lu, Rev. Adv. Mater. Sci. **5**, 72 (2003)